Modified capillary number to standardize droplet generation in suction driven microfluidics

Jatin Panwar

jatin.panwar@epfl.ch

École Polytechnique Fédérale de Lausanne (EPFL)

Rahul Roy

Indian Institute of Science Bangalore

Research Article

Keywords: Microfluidics, Capillary number, droplet generation, suction pressure control, microchannel geometry

Posted Date: November 13th, 2023

DOI: https://doi.org/10.21203/rs.3.rs-3583995/v1

Additional Declarations: No competing interests reported.

Version of Record: A version of this preprint was published at Microfluidics and Nanofluidics on March 22nd, 2024. See the published version at https://doi.org/10.1007/s10404-024-02714-2.

Modified capillary number to standardize droplet generation in suction driven microfluidics

Jatin Panwar [1,2,#] and Rahul Roy [1,#]

[1] Department of Chemical Engineering, Indian Institute of Science (IISc), India

[2] Institute of Bioengineering, School of Engineering, École Polytechnique Fédérale de Lausanne (EPFL), Switzerland

Correspondence: jatin.panwar@epfl.ch, rahulroy@iisc.ac.in

Abstract:

In droplet microfluidic devices with suction-based flow control, the microchannel geometry and suction pressure at the outlet govern the dynamic properties of the two phases that influence the droplet generation. Therefore, it is critical to understand the role of geometry along with suction pressure in the dynamics of droplet generation to develop a predictive model. We conducted a comprehensive characterization of droplet generation in a flow focusing device with varying control parameters. We used these results to formulate a scaling argument and propose a governing parameter, called as modified capillary number (Ca_L), that combines normalized droplet volume with geometrical parameters (length of dispersed and continuous phase channels) and flow parameters (interfacial tension, phase viscosity and velocity) in a power-law relationship. Ca_L effectively captures the transition from squeezing and dripping regimes of droplet generation, providing essential insights into the design requirements for suction-driven droplet generation. These findings are key to standardize microfluidic flow-focusing devices that can achieve the desired droplet generation behavior with optimal pressure consumption.

Keywords: *Microfluidics, Capillary number, droplet generation, suction pressure control, microchannel geometry.*

1. INTRODUCTION

Since its advent, droplet microfluidics is consistently evolving into a major technique for high throughput bio analysis and chemical synthesis [1–5]. Droplet generation requires two immiscible fluids that act as a continuous phase and a dispersed phase. The two phases are carried in separate channels and are made to interact at a junction where they make an interface. Further fluid interaction causes the interface to deform under the shear stresses that initialize interfacial instabilities and finally result into continuous phase pinching off a drop of dispersed phase in a continuous fashion[6,7]. Conventionally, these fluids are pumped into the microchannels either by i) mechanical pressure (using pressure controllers or hydrostatic heads)[8] or ii) positive displacement of fluid (using syringe pumps)[9]. These methods not only provide a fine control over the flow rates of individual streams but also maintain the high pressures required during such fluid-flow operations. However, these methods come with some limitations. The cost associated with the two mentioned methods is considerably high and they also have a large footprint that hampers the mobility of the device. This in-turn reduces their applicability as point of care and diagnostic devices. The high reagent volumes required in these methods can also be a problem when using costly or limited reagents. The high pressures that accumulates within the channel during operation challenge the bonding of the fabricated layers and sometimes results in delamination and leaks in the device. Lastly, with multiple parameters to control, such devices require trained personals or high level of instrumentation control at some point of operation.

In this work, we characterized and optimized suction-based microfluidics as an accessible and significantly economical method for droplet generation to overcome the limitations of conventional microfluidic approach. The basic requirements for any microfluidic droplet generation device are: i) Driving force that induces the fluid-flow and ii) a specific ratio between the flow rates of continuous and dispersed phase that insures the droplet generation[9]. In this study, we use negative pressure or suction through the exit as the driving force for all operations, and control the flow rate ratio by the geometry of the primary channels i.e. the inlet channels[10,11]. The suction is generated by the feedback-controlled pull-back of an empty syringe that generated enough suction pressure to drive the flow of dispersed and continuous phases. The geometry of the device enables the two fluids to interact at the required flow rate ratios resulting in droplet generation.

The primary objective of this study is to identify a governing parameter that can define droplet volume and the droplet generation regime as a function of control variables. These variables include device geometry (length of dispersed and continuous phase inlet channels), fluid properties (viscosity of both phases and interfacial tension) and flow properties (velocity of phases before flow focusing junction). Such a governing parameter can help standardize flow-focusing droplet generator as a unit operation. The study also serves as a prerequisite to design suction driven microfluidic devices with multiple unit operation where available suction pressure (limited to ~100 kPa) and each integrated operation has to be optimized for its pressure consumption. As flow-rate control in individual channels is not possible in suction-based microfluidic platforms, characterizing droplet generation as a unit operation becomes pertinent.

Controlled droplet generation has many industrial applications and hence it has been extensively studied to understand droplet generation dynamics and its relation with flow parameters. To understand the droplet pinch-off in microfluidic channels, it is important to examine the local viscous stresses and the dynamic pressure field surrounding the emerging droplet. A few dimensionless numbers are used to express the relationship between viscous stresses and pressure fields. Most common among them is the capillary number (*Ca*) which characterizes the ratio of viscous stresses and capillary pressure.

$$Ca = \frac{\mu_C Gn}{\gamma} = \frac{\mu_C V_C}{\gamma} \quad (1)$$

Here *G* is the characteristic rate of strain and *n* is the characteristic size of the neck before the pinch-off[12]. The subscripts *D* and *C* are used to represent dispersed and continuous phase respectively. The other important dimensionless numbers are the viscosity ratio (λ) and flow rate ratio (φ).

$$\lambda = \frac{\mu_D}{\mu_C} \quad (2)$$

$$\varphi = \frac{Q_D}{Q_C} \quad (3)$$

Based on these fundamentals, there have been a few efforts to capture droplet volume mathematically. The earlier studies stated that droplet are formed when viscous stresses overcome the interfacial tension or when *Ca* tends to unity where the droplet diameter (*d*) was expressed as follows[13]:

$$d \sim \frac{2\sigma}{\mu_C \epsilon} \quad (4)$$

Here, ϵ is the shear rate within the junction. The expression did not consider the relation between flow rates of the different phases. The subsequent studies provide a model to predict the droplet-size-based on the force balance (Eq. 5 and 6)[14]. It should be noted that the authors did not account for the viscous stresses from the dispersed phase that contributes to the resistance to deformation along with the interfacial tension.

$$d^{*4} - 2d^{*3} + \frac{\omega}{2} d^{*2} + \frac{\alpha}{2C_\lambda Ca} = 0 \quad (5)$$

$$C_\lambda = \frac{3 + 2\lambda}{1 + \frac{1}{\lambda}} \quad (6)$$

Here, $d^* = d/D_C$ is the droplet diameter scaled by continuous phase channel's hydraulic diameter, α is the ratio of effective cross section area of two channels, C_λ is the correction factor incorporating the viscosity ratio and ω represents the ratio of droplet velocity to the average velocity of the continuous phase. The model predicts that the droplet size is only a function of capillary number and is independent of flow rate ratio. The model however, does not report a strong quantitative agreement (limited to ~ 25 %) with the experimental findings[15]. Even with these different considerations and hypothesis, both of the discussed models agree on the point that droplet pinch-off in a cross-flow geometry is dominated by the viscous drag in the dripping regime. Squeezing regime, on the other hand, is defined by the intervention of geometry[16,17]. It was found that in squeezing regime, the droplet volume (*v*) is a strong function of geometry and capillary number[18].

$$v = v_{C,ref} Ca^m + t_{n,ref} Ca^n Q_D \quad (7)$$

Here, v_c is the droplet volume before the breaking is initiated and t_n is the time between initiation of breaking and collapse of neck. $v_{c,ref}$ and $t_{n,ref}$ are calculated at *Ca* = 1 and *n* and *m* are channel geometry dependent parameters. Even though this model accounts for dispersed phase flow rate, without the inclusion of viscosity ratio, it cannot account for the viscosity of dispersed phase. These models indicated that increasing the viscosity of the continuous phase

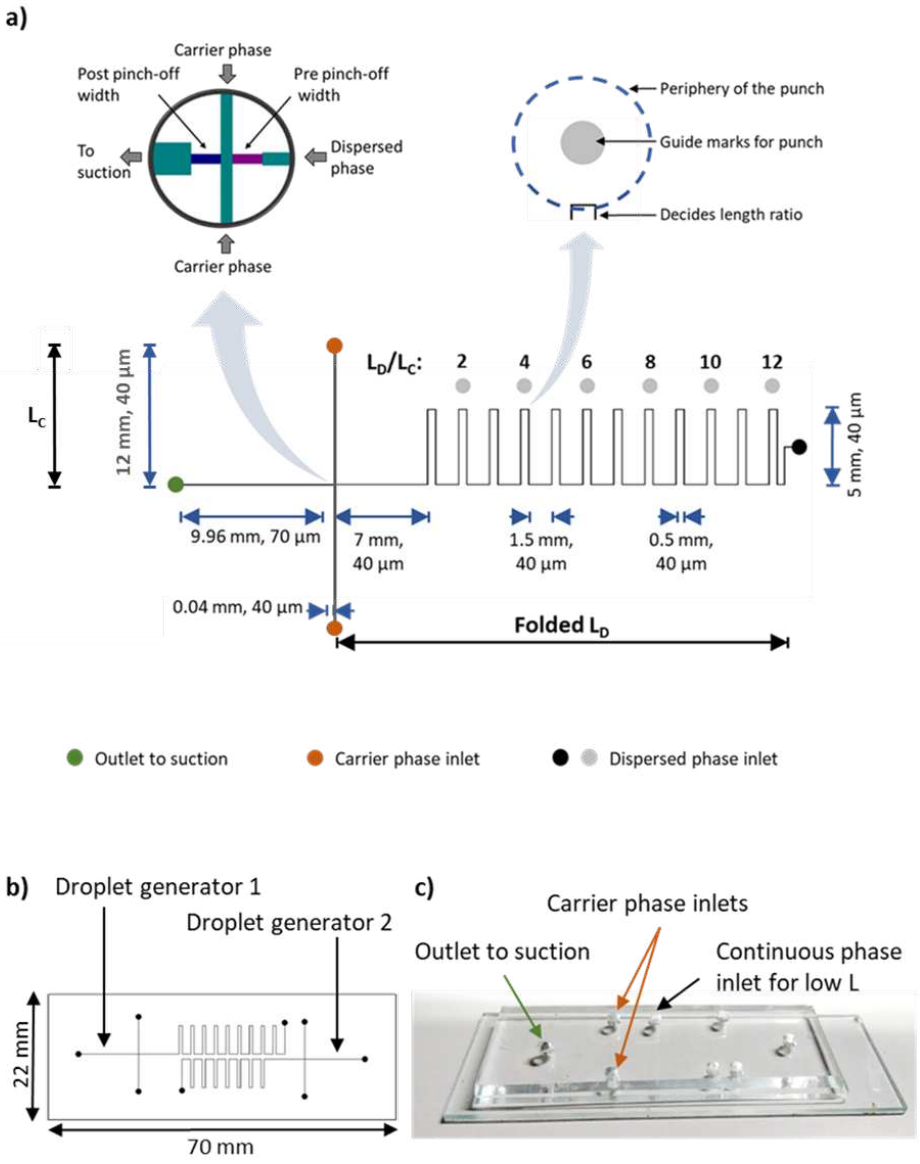

Figure 1. *Device architecture. a) Schematic of the microfluidic droplet generator standardized to be used with suction microfluidics. b**)** The geometry for the droplet generator device used for photolithography. c) PDMS microfluidic chip.*

liquid results in decreased droplet size especially in dripping regime due to increased viscous drag and thus shear forces on the interface[14,15]. It was also found that at a viscosity ratio of ~1, the transition from dripping to squeezing regime occurs at Ca ~ 0.015 [19]. In another model, it was proposed that droplet volume (V) and droplet diameter (d) depends upon continuous phase flow rate (Q_C) and capillary number when dispersed phase flow rate is constant (Eq. 8 and 9)[20]. According to this model, the transition from squeezing regime is a function of microchannel dimension.

$$V \propto \frac{1}{\mu_C Q_C} \tag{8}$$

$$d \propto Ca^{-\frac{1}{3}} \tag{9}$$

However, these models lack the contribution from the dispersed phase viscosity and velocity in droplet generation. In our study, we attempted to identify and incorporate the role of dispersed phase viscosity and flow rate in the interfacial dynamics of droplet generation in microfluidic devices. To standardize droplet generation in suction microfluidics, we provide a simple yet effective model that outlines the design and driving force requirements for droplet generation and its corresponding regimes.

2. METHODS

2.1. Device architecture

We designed a modular flow-focusing device using photolithography that can generate droplets over a wide range of dispersed and continuous phase flow

rate ratios[21,22] (20, 21). Since by design, these flow rates are determined by the length of the channels, we defined length ratio (L) as the ratio of length of inlet channel for dispersed phase (L_D) to the length of inlet channel for continuous phase (L_C).

	Water	Glycerol	HFE 7500	1-Octanol
Viscosity (m.Pa.s)	0.89	1412	1.3	7.36
Density (kg/m³)	1000	1260	1614	869

Table 1. *Viscosity and density of fluids used in the characterization.*

	Dispersed phase	Continuous phase	Interfacial surface twnsion (mN/m)	Viscosity ratio ($\lambda = \mu_D/\mu_C$)
System 1	Water	HFE-7500 with surfactants	5.67	0.68
System 2	Water	1-Octanol with surfactants	3.923	0.12
System 3	Glycerol	HFE-7500 with surfactants	2.032	1086.15

Table 2. *Systems used in characterization defined by the dispersed and continuous phase along with their respective Interfacial tension and viscosity ratio.*

Based on our design, apart from the applied suction pressure, length ratio is the only other control parameter that defines the dispersed phase – continuous phase interaction. As pressure drop (ΔP) across a channel is proportional to its length, the volumetric flow rate and fluid viscosity (μ); for similar area of cross section, at any given ΔP, the length ratio defines geometric properties as well as the interdependent flow properties within that channel (Eq. 10 and 11)[23]. If the pressure at the pinch-off junction is P_J and inlets of both continuous and dispersed phase channel are kept at P_{atm}, the pressure-drop in both channels (ΔP_D and ΔP_C) will be same ($P_{atm} - P_J$) and thus length ratio can be written as:

$$\frac{\Delta P_D}{\Delta P_C} = \frac{L_D \mu_D Q_D}{L_C \mu_C Q_C} \tag{10}$$

For $\Delta P_D = \Delta P_C = P_{atm} - P_J$

$$L = \frac{L_D}{L_C} = \frac{\mu_C Q_C}{\mu_D Q_D} \tag{11}$$

In our device, the total length of continuous phase channel is kept constant at 12 mm but the length of dispersed phase can be varied between 12 to 72 mm. The range of length ratio (L) thus, can vary from 1 to 12. To accommodate the large length of the dispersed phase channel, we folded the channel by incorporating 90° bends (**Figure 1a**). The contribution of these bends to the pressure losses within the channel is not accounted as these losses are insignificant in non-inertial flown at low Reynolds number[24]. The channel carries 12 distinct equidistant turns with visible guide marks on top of it that can be used to punch an inlet hole at desired length. The channels meet at the pinch-off junction and converge to the exit channel that has a 40 µm wide and 40 µm long post pinch-off neck connected to a 70 µm wide and 10 mm long channel ending into the exit port (**Supplementary information S.1**). We incorporated two independent microfluidic droplet generators with a footprint of 2.2 cm x 7 cm casted over a plain and thin PDMS layer on a glass slide (**Figure 1**). The thin PDMS layer ensures uniform surface properties within the microchannels.

2.2 Device operation

We selected three pairs of dispersed and continuous phases for a comprehensive characterization of the suction driven microfluidic droplet generator in terms of evolution of droplet volume with fluid properties. The phase pairs were chosen to provide a wide range of fluid properties, namely, interfacial surface tension and viscosity. Three fluids combinations were DI water in HFE 7500, Glycerol in HFE 7500 and DI water in 1-Octanol. We used a commercial variant of HFE 7500 which was premixed with surfactants (BIORAD #1863005) while 2 wt % span 80 was added to 1-Octanol as surfactant[25]. The contributing properties of all the phases and systems are shown in **Table 1** and **Table 2**. We generated the droplets at six discrete and equidistant length ratios (2 to 12) and at ten equidistant values of volume swept from the suction syringe (0.1 to 10 mL) corresponding to applied suction pressure of 2.3 to 23 kPa via a custom made suction pressor control software (**Supplementary information S.2, Supplementary software S1**). After establishing the stability of droplets generated using suction, we measured the volume and frequency of the droplets (averaged over 100 droplets) generated for each experiment and studied the effect of applied pressure and fluid properties that will be discussed in forthcoming sections (**Supplementary information S.3**).

3. RESULTS AND DISCUSSION

3.1. Effect of pressure

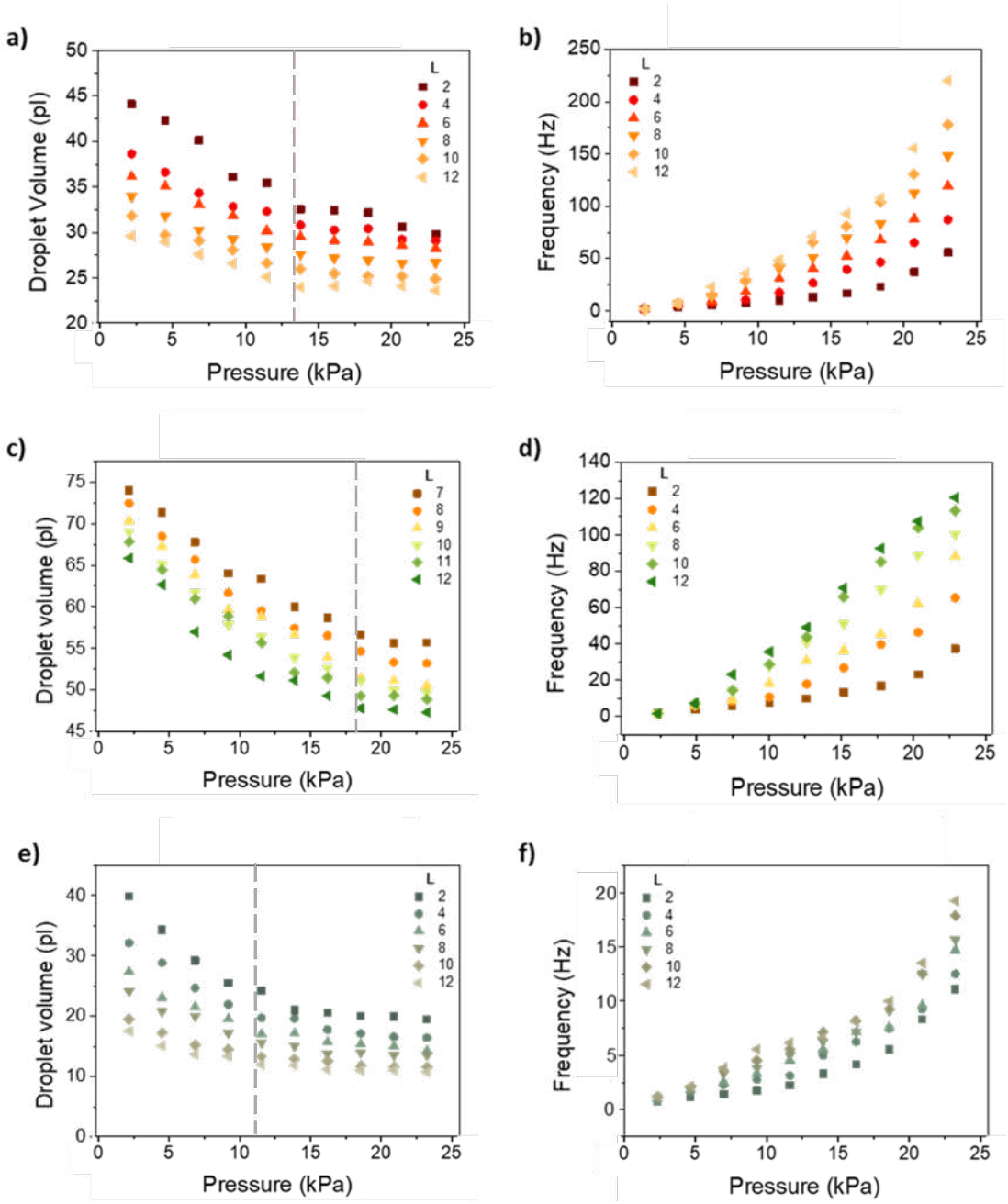

Figure 2: *Droplet volume and frequency generated as a function of increasing suction pressure as measured in: a and b) System 1: water in HFE 7500. c and d) System 2: water in octanol. e and f) System 3: glycerol in HFE 7500. The vertical dashed line shows the regime transition and its corresponding suction pressure.*

For all the systems, the droplet volume decreased with the increasing suction pressure while the frequency increased (**Figure 2**). However, the decrease in volume and frequency-rise was not linear with the applied suction. The volume decreased at a faster rate at low pressures and at high pressures, the volume change was lower. On the other hand, the frequency increased slowly at low pressures and the change in frequency got steeper as pressure increases. The dominating parameter in droplet generation is the viscous drag from the continuous phase, which increases linearly with the applied suction pressure, and results in an almost linear drop in droplet volume. This is consistent with the apparent linear drop in higher droplet volumes observed at low length ratios for fixed viscosity ratios. However, this apparent linear drop was observed only at low pressure drops (<10 kPa). As we increased the pressure drop, the droplet volume appeared to stay constant as was observed in all three systems. From these results, it can be stated that droplet volume is most sensitive to applied pressure at low pressure and this sensitivity decreases with increasing pressure. These distinct behaviors also correspond to two separate regimes of droplet generation.

The discontinuity observed in the droplet volume with increasing applied pressure in all the three systems

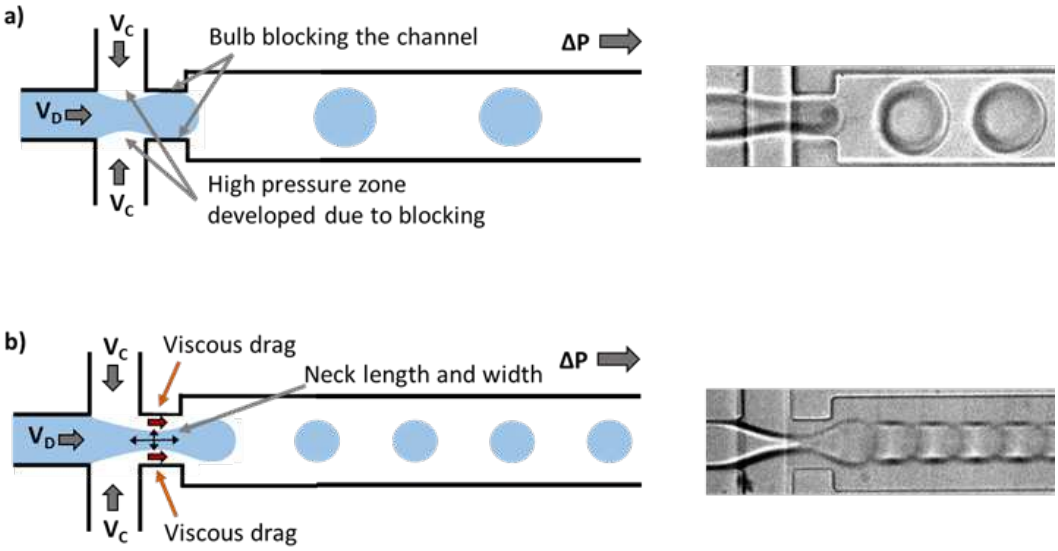

Figure 3: *a) Schematic and optical image representing squeezing regime. b) Schematic and optical image representing dripping regime.*

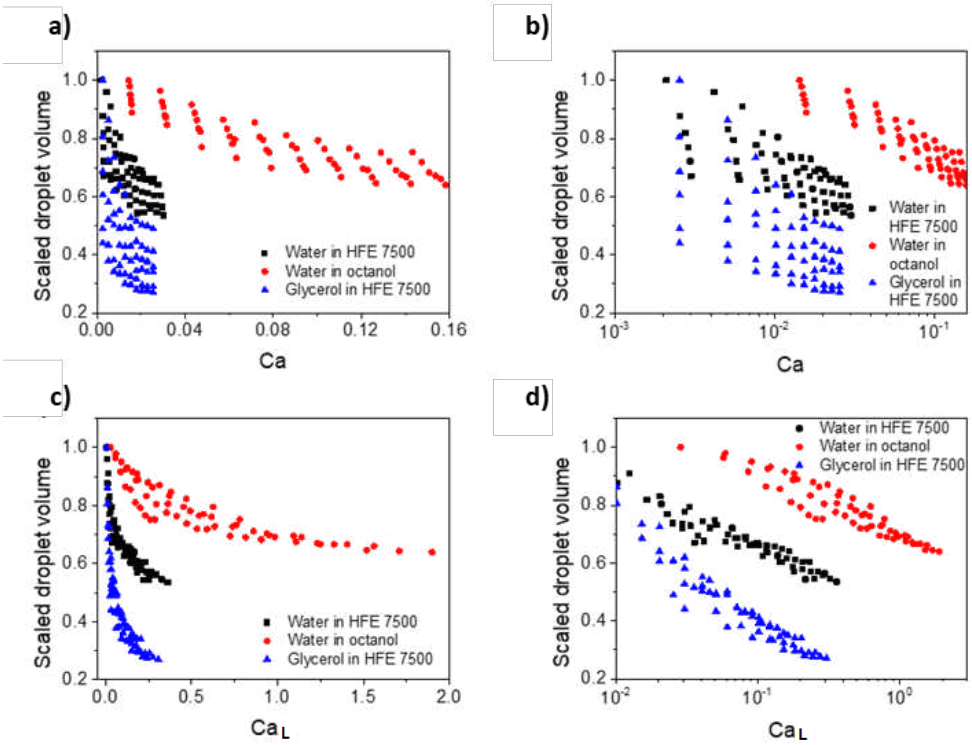

Figure 4: *a and b) Scaled droplet volume as a function of capillary number in linear and log_{10} scale for all three systems. c and d) Scaled droplet volume as a function of modified capillary number in linear and log_{10} scale for all three systems.*

(**Figure 2 a, c and e**) can be attributed to the effect of geometry and can be used to define the transition between squeezing and dripping regime. A visual inspection confirms the role of interaction between dispersed phase and the channel walls in controlling the regime transformation (**Figure 3**). Just before the pinch-off, the dispersed phase develops a *bulb* followed by a *neck.* As the bulb grows, it touches the side-walls of the microfluidic channel and blocks the flow of continuous phase into the exit channel that causes two physical changes at the interface (**Figure 3**). First, there is a sudden increase in the pressure due to the blockage that forces the neck to stretch. Second, due to sudden change in pressure the normal shear stress applied by the continuous phase increases compressing the neck. Both these factors result into droplet pinch off into volumes that decrease in proportion to the applied suction pressure as well as continuous phase flow rate contributing to a sharp fall in droplet volume with increasing applied pressure. However, as the applied suction pressure increases, the bulb size reduces and it no longer touches the channel walls that results in the observed discontinuity and the onset of *dripping regime* (**Figure 3b**).

3.2 Effect of viscosity

We observed interesting effects on the droplet volume with the change in dispersed and continuous phase viscosities. When the viscosity of continuous phase was increased, it is intuitive to think that the increased viscous forces would result in small droplet volumes. However, with increased viscosity, the flow rate of the continuous phase reduces proportionally which counters the effect of viscosity change. Moreover, the reduced flow rate of continuous phase further results in a proportional increase in the dispersed phase flow rate that finally resulted in droplets of higher volume. Hence, we observed higher droplet volume for system 2 where the viscosity of dispersed phase was highest in comparison to system 1 and 3 (**Figure 2**).Similarly, a higher viscosity of dispersed phase should result in droplets of higher volume in case of flow rate driven flows[26]. Contrary to this, in suction microfluidics, the dispersed phase viscosity did not contribute significantly in changing the droplet volume. This is because the increased viscous forces from the dispersed phase are compensated by the proportional increase in the flow rate of continuous phase. This explains why the droplet volumes observed in system 1 and system 3 are similar even with a dispersed phase viscosity difference of the order of 10^3 **(Figure 2 a and e**). Similarly, the effect of proportional decrease in the dispersed phase flow rate can be seen in the decrease in the generation frequency for system 3.

3.3. Droplet volume characterization

From the previous discussions, we know that the regime with least volume sensitivity is observed at high suction pressure. However, even though the droplet volume is consistent in this regime, a unit operation working at a regime that requires high pressure is not recommended especially because of the limited available pressure in suction microfluidics. There should be an optimal range where the sensitivity is not compromised with high pressure drop. Therefore, it is pertinent to identify and represent this optimal regime with a dimensionless parameter. To estimate this empirically, we first calculated the flow parameters for each system that includes flow rate and velocity of both phases in respective channels. These parameters were then used to calculate the Reynolds number and capillary number for the respective phases (**Supplementary figure S7-S9**). Capillary number (*Ca*) is conventionally used to predict droplet behavior as it reflects the balance between shear and interfacial forces that influences droplet pinch-off [2,26–28]. We explored the relation between capillary number and droplet volume to explore this correlation. The analysis showed that the distribution of droplet volume is wide; in other words, no strong correlation of droplet volume was found with *Ca* (**Figure 4 a and b**). We argue this is because *Ca* does not account for flow properties of dispersed phase like velocity (or flow rate) and viscosity. As in suction microfluidics, the flow properties in individual channels are intertwined with the geometrical properties, a particular *Ca* value may not represent droplets generated with any length ratio. To have a governing parameter that includes interaction between the two phases along with their individual properties, we combined the capillary number (defined by continuous phase) with the length ratio and called it as *modified capillary number* (Ca_L). Interestingly, we observed a strong correlation of droplet volume with Ca_L with narrower distributions of droplet volume (**Figure 4 c and d**). This behavior can be understood in detail once we describe the physical significance of Ca_L.

3.4. Modified Capillary Number (Ca_L)

We define the modified capillary number as the product of capillary number and length ratio (*L*) (Eq. 2.14). For suction microfluidics, the length ratio not only signifies the geometrical aspect of the device, but also the relative strength of viscous and shear forces between dispersed and continuous phase. The capillary number defines the relative dominance of viscous forces due to continuous phase, relative to interfacial surface forces lacking the effect of viscous forces due to dispersed phase. Whereas, Ca_L written as the ratio of capillary number and inversed length ratio signifies the ratio of viscous forces from continuous phase and the viscous forces due to dispersed phase

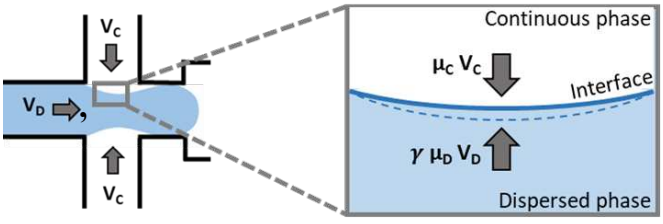

Figure 5: *Schematic of viscous, shear and surface force components acting on the interface at the neck during pinch-off.*

along with the interfacial tension (Eq. 2.16 and 2.17). At the interface of the two phases, the normal shear stress due to viscous forces of continuous phase tries to deform the interface towards the dispersed phase, while the normal shear stress due to viscous forces from dispersed phase and interfacial tension tries to resist this deformation (**Figure 5**). Thus, *modified capillary number or Ca_L is a dimensionless number that describes the relative dominance between the tendency of continuous phase to deform the interface and tendency of dispersed phase along with interfacial tension to resist the deformation.*

$$Ca_L = Ca.L = Ca.\frac{L_D}{L_C} \tag{12}$$

$$Ca_L = \frac{Ca}{\frac{L_C}{L_D}} \tag{13}$$

$$Ca_L = \frac{\frac{\mu_C V_C}{\gamma}}{\frac{\mu_D V_D}{\mu_C V_C}} \tag{14}$$

$$Ca_L = \frac{{\mu_C}^2 {V_C}^2}{\gamma \mu_D V_D} \tag{15}$$

$$Ca_L = \frac{Deformative\ forces\ on\ the\ interface}{Restoring\ forces\ on\ the\ interface}$$

At low Ca_L values, the dispersed phase and interfacial tension resist the deformation and delays the pinch off, resulting in a droplet of high volume generated at low frequency. Similarly, at high values of Ca_L, the continuous phase deforms the interface more efficiently resulting in droplets of lower volume generated at a higher frequency. The observed trends agree with this argument for all the systems with different viscosity and interfacial tensions (**Figure 4 c and d**).

There are three key observations from the droplet volume distribution as a function of Ca_L (**Figure 4 c and d**). First, the transition between regimes is similar for systems with similar continuous phase (at $Ca_L \sim 10^{-1}$ for system 1 and 3) independent of their viscosity and length ratios. This explains why Ca_L is more useful than Ca when it comes to defining droplet volume distribution for suction microfluidics. Second, droplet volume tends to vary less at high values of Ca_L for all systems. And third, the values of the seemingly constant droplet volume differ for each system; highest in system 2 and lowest in system 3. To explain the latter two observations, we have to understand the effect of the curvature and interfacial tension on the energy required to bend the interface. This theory was first developed by J. Willard Gibbs, that explains the work done in deforming (stretching ($\delta\alpha$), bending (δH), torsion (δD)) a surface element (ΔA)[29]. The relationship is defined as:

$$\delta W_S = \gamma\delta\alpha + B\delta H + \theta\delta D \tag{16}$$

$$\delta\alpha = \delta\frac{(\Delta A)}{\Delta A} \tag{17}$$

$$B, \theta = f(\gamma) \tag{18}$$

Here, δW_S is the work done per unit area, γ is the surface energy per unit area (i.e. interfacial tension) and B and ϑ are called bending and torsion moments respectively. $\delta(\Delta A)/\Delta A$ is the change in the area of surface element due to stretching which can be considered as constant during the pinch-off process. Similarly, the torsion element of the equation is considered insignificant due to absence of any rotational force.

As the droplet volume decreases with increasing Ca_L, the energy required to bend the interface (δW_S) to pinch further smaller droplet increases. This required work-done thus grows with Ca_L. The net energy supplied by the fluids to bend the interface is proportional to the viscous forces due to continuous phase and thus rise linearly with Ca_L. Following these two arguments, it is clear that as Ca_L increases, the energy required to further reduce the droplet size balances the energy supplied by viscous forces resulting in droplets of constant volume. This argument explains why droplet volume tends to decrease less at high Ca_L. In addition, as δW_S is a function of interfacial tension (γ), with higher γ, minimum droplet volume increases. This explains why the minimum droplet volume is higher in system 1 and 2 as compared to system 3 and why it is similar in system 1 and 2 (**Figure 4 c and d**). Therefore, we can fit the behavior of different systems (in terms of droplet volume scaled with channel width (w) in that system) with increasing Ca_L. The linearity observed in the droplet volume as a function of log (Ca_L) indicates a relationship that follows inverse power law (**Figure 4 d**). In general, the scaled droplet volume ($\bar{V}_{Drop}$) is inversely proportional to Ca_L. The fitted function is as follows:

$$\bar{V}_{Drop} = \frac{V_{Drop}}{w^3} \tag{19}$$

$$\bar{V}_{Drop} \propto \frac{1}{{Ca_L}^b} \quad (20)$$

$$\bar{V}_{Drop} = \frac{a}{{Ca_L}^b} \quad (21)$$

$$a \propto \frac{\mu_C}{B} \quad (22)$$

Here, a is the proportionality constant that is a function of continuous phase viscosity (μ_c) and bending moment (B). The bending moment also accounts for the channel dimension, i.e., higher the channel width, lower will be the bending moment[29]. The observation shows excellent fit with the function represented in equation 21 when b = 0.14 (**Figure 6**). Relationships for each system can be written as:

$$\bar{V}_{Drop,System\ 1} = \frac{0.32}{{Ca_L}^{0.14}} \quad (23)$$

$$\bar{V}_{Drop,System\ 2} = \frac{0.69}{{Ca_L}^{0.14}} \quad (24)$$

$$\bar{V}_{Drop,System\ 3} = \frac{0.29}{{Ca_L}^{0.14}} \quad (25)$$

The similarity between system 1 and 3 validates that a is a function of the viscosity of continuous phase, which were kept same in both systems while their dispersed phase viscosities differed by an order of 10^3 (Eq. 23 and 25). This exercise proves that Ca_L defines the relationship between fluid properties, device geometry (L) and volume of droplet generated in a flow focusing microfluidic device. Equations 23 to 25 can be used to identify droplet generation regimes with Ca_L. A low Ca_L represents squeezing regime of droplet generation with high droplet volume sensitivity and low-pressure consumption. On the other hand, dripping regime is observed at high Ca_L values that signifies low droplet volume sensitivity and high generation efficiency and pressure consumption. The transition between squeezing to dripping regime corresponds to the change in slope and was observed at $Ca_L \sim 10^{-1}$ for all systems.

4. CONCLUSION

We have characterized a suction-based microfluidic droplet generator on the basis of volume of droplets generated with varying geometrical and control parameters using three pairs of dispersed and continuous phases. We have consistently observed and

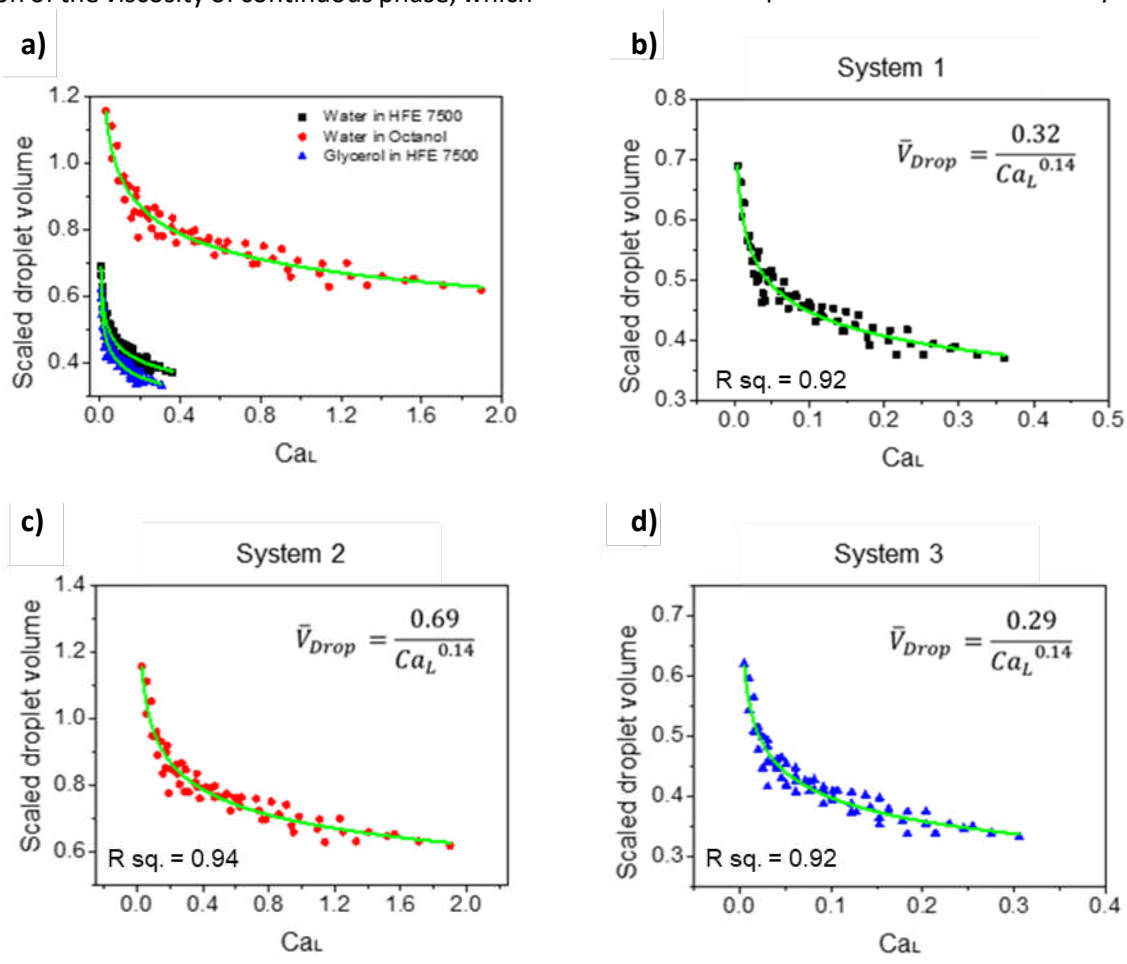

Figure 6: *a) Inverse power law fit for scaled droplet volume with Ca_L for all three systems. b-d) The fitted function represented for each system.*

reported that in suction microfluidics, the droplet volume is independent of the dispersed phase viscosity. We defined a dimensionless number as modified capillary number (Ca_L) elucidating the relative dominance of deformative and restoring forces acting on the interface between dispersed and continuous phase at the interface. We found a strong correlation between droplet volume scaled by the microchannel width and modified capillary number as $\bar{V}_{Drop} \propto Ca_L^{-0.14}$. We also used this relationship between droplet volume and Ca_L to define droplet generation regimes with $Ca_L \sim 10^{-1}$ as the transition point from squeezing to dripping regime. We suggest a narrow range of $0.1 < Ca_L < 0.2$ as an optimized regime, i.e. low droplet volume sensitivity and pressure consumption but high generation frequency.

Along with flow properties, the Ca_L also accounts for length ratio as a geometrical parameter. Thus, Ca_L is expected to serve as realistic design parameter that defines channel geometry for future suction microfluidics-based droplet generation devices.

Symbols:

Ca_L	*Modified capillary number*
Ca	*Capillary number*
μ_C	*Viscosity of continuous phase*
μ_D	*Viscosity of dispersed phase*
G	*Characteristic rate of strain*
n	*characteristic size of neck*
V_D	*Velocity of dispersed phase*
V_C	*Velocity of continuous phase*
γ	*Interfacial tension*
λ	*Viscosity ratio*
φ	*Flow rate ratio*
Q_D	*Dispersed phase flow rate*
Q_C	*Continuous phase flow rate*
d	*Droplet diameter*
ϵ	*Shear rate*
ω	*Droplet velocity/average cont. phase velocity*
C_λ	*Correction factor*
v	*Droplet volume*
α	*Ratio of effective cross section area of channels*
t_n	*time between initiation and breakup*
ΔP_D	*Pressure drop in dispersed phase channel*
ΔP_C	*Pressure drop in continuous phase channel*
P_{atm}	*Absolute atmospheric pressure*
P_j	*Absolute pressure at the junction*
L_D	*Length of dispersed phase channel*
L_C	*Length of continuous phase channel*
L	*Length ratio*
δW_S	*Work done per unit area*
$\delta\alpha$	*Work done by stretching*
δH	*Work done by bending*
δD	*Work done by torsion*
ΔA	*Surface element*
B	*Bending moments*
ϑ	*Torsion moment*
$\bar{V}_{Drop}$	*Observed droplet volume*
$\bar{V}_{Drop}$	*Scaled droplet volume*

Supplementary Information: The online version contains supplementary material available at xxxxxxxxxxxxxx. The supplementary software S1 for suction pressure control is available at: doi.org/10.5281/zenodo.10031121

Acknowledgements: This project was partially funded by support from the Indian Institute of Science (IISc) Bangalore, DBT Biodesign Bioengineering Initiative (BT/PR13926/MED31/97/2010) and Rao Biomedical Research Fund (RBRF02). We also acknowledge use of the photolithography facilities at the Center for Nano Science and Engineering (CeNSe), funded by the Department of Information Technology, Gov. of India.

Author contributions: JP and RR designed the experiments. JP conducted the experiments and wrote the manuscript. Both authors reviewed the manuscript.

Data availability: Experimental data presented in his study is available upon request to the authors.

Conflict of interest: There is no conflict of interest.

References

1. Song H, Chen DL, Ismagilov RF. Reactions in Droplets in Microfluidic Channels. *Angew Chem Int Ed*. 2006;45(44):7336-7356. doi:10.1002/anie.200601554
2. Teh SY, Lin R, Hung LH, P. Lee A. Droplet microfluidics. *Lab on a Chip*. 2008;8(2):198-220. doi:10.1039/B715524G
3. Lagus TP, Edd JF. A review of the theory, methods and recent applications of high-throughput single-cell droplet microfluidics. *J Phys D: Appl Phys*. 2013;46(11):114005. doi:10.1088/0022-3727/46/11/114005
4. Chou WL, Lee PY, Yang CL, Huang WY, Lin YS. Recent Advances in Applications of Droplet Microfluidics. *Micromachines*. 2015;6(9):1249-1271. doi:10.3390/mi6091249
5. Zhao CX. Multiphase flow microfluidics for the production of single or multiple emulsions for drug delivery. *Advanced Drug Delivery Reviews*. 2013;65(11):1420-1446. doi:10.1016/j.addr.2013.05.009

6. Christopher GF, Anna SL. Microfluidic methods for generating continuous droplet streams. *J Phys D: Appl Phys*. 2007;40(19):R319. doi:10.1088/0022-3727/40/19/R01
7. Liu H, Zhang Y. Droplet formation in microfluidic cross-junctions. *Physics of Fluids*. 2011;23(8):082101. doi:10.1063/1.3615643
8. Bong KW, Chapin SC, Pregibon DC, Baah D, Floyd-Smith TM, Doyle PS. Compressed-air flow control system. *Lab Chip*. 2011;11(4):743-747. doi:10.1039/C0LC00303D
9. Zhu P, Wang L. Passive and active droplet generation with microfluidics: a review. *Lab Chip*. 2016;17(1):34-75. doi:10.1039/C6LC01018K
10. Abate AR, Weitz DA. Syringe-vacuum microfluidics: A portable technique to create monodisperse emulsions. *Biomicrofluidics*. 2011;5(1):014107. doi:10.1063/1.3567093
11. Panwar J, Roy R. Integrated Field's metal microelectrodes based microfluidic impedance cytometry for cell-in-droplet quantification. *Microelectronic Engineering*. 2019;215:111010. doi:10.1016/j.mee.2019.111010
12. Stone HA. Dynamics of Drop Deformation and Breakup in Viscous Fluids. *Annual Review of Fluid Mechanics*. 1994;26(1):65-102. doi:10.1146/annurev.fl.26.010194.000433
13. Thorsen T, Roberts RW, Arnold FH, Quake SR. Dynamic Pattern Formation in a Vesicle-Generating Microfluidic Device. *Phys Rev Lett*. 2001;86(18):4163-4166. doi:10.1103/PhysRevLett.86.4163
14. Husny J, Cooper-White JJ. The effect of elasticity on drop creation in T-shaped microchannels. *Journal of Non-Newtonian Fluid Mechanics*. 2006;137(1):121-136. doi:10.1016/j.jnnfm.2006.03.007
15. Xu JH, Li SW, Tan J, Wang YJ, Luo GS. Preparation of highly monodisperse droplet in a T-junction microfluidic device. *AIChE Journal*. 2006;52(9):3005-3010. doi:10.1002/aic.10924
16. Garstecki P, J. Fuerstman M, A. Stone H, M. Whitesides G. Formation of droplets and bubbles in a microfluidic T-junction—scaling and mechanism of break-up. *Lab on a Chip*. 2006;6(3):437-446. doi:10.1039/B510841A
17. Garstecki P, Stone HA, Whitesides GM. Mechanism for Flow-Rate Controlled Breakup in Confined Geometries: A Route to Monodisperse Emulsions. *Phys Rev Lett*. 2005;94(16):164501. doi:10.1103/PhysRevLett.94.164501
18. Van der Graaf S, Nisisako T, Schroën C, Van Der Sman R, Boom R. Lattice Boltzmann simulations of droplet formation in a T-shaped microchannel. *Langmuir*. 2006;22(9):4144-4152.
19. De Menech M, Garstecki P, Jousse F, Stone HA. Transition from squeezing to dripping in a microfluidic T-shaped junction. *journal of fluid mechanics*. 2008;595:141-161.
20. Lee W, Walker LM, Anna SL. Role of geometry and fluid properties in droplet and thread formation processes in planar flow focusing. *Physics of Fluids*. 2009;21(3).
21. Thompson LF. An introduction to lithography. In: ACS Publications; 1983.
22. Duffy DC, McDonald JC, Schueller OJ, Whitesides GM. Rapid prototyping of microfluidic systems in poly (dimethylsiloxane). *Analytical chemistry*. 1998;70(23):4974-4984.
23. Gooch JW. *Encyclopedic Dictionary of Polymers*. Vol 1. Springer Science & Business Media; 2010.
24. Pantokratoras A. Steady laminar flow in a 90 bend. *Advances in Mechanical Engineering*. 2016;8(9):1687814016669472.
25. Xu J, Li S, Lan W, Luo G. Microfluidic approach for rapid interfacial tension measurement. *Langmuir*. 2008;24(19):11287-11292.
26. Wehking JD, Gabany M, Chew L, Kumar R. Effects of viscosity, interfacial tension, and flow geometry on droplet formation in a microfluidic T-junction. *Microfluidics and nanofluidics*. 2014;16:441-453.
27. Tice JD, Song H, Lyon AD, Ismagilov RF. Formation of droplets and mixing in multiphase microfluidics at low values of the Reynolds and the capillary numbers. *Langmuir*. 2003;19(22):9127-9133.
28. Baroud CN, Gallaire F, Dangla R. Dynamics of microfluidic droplets. *Lab on a Chip*. 2010;10(16):2032-2045.
29. Gibbs JW. *The Scientific Papers: Dynamics Vector Analysis and Multiple Algebra Electromagnetic Theory of Light, Etc*. Vol 2. Longmans, Green and Company; 1906.

Supplementary Files

This is a list of supplementary files associated with this preprint. Click to download.

- SupplementaryinfoPanwarandRoy2023.pdf